Monthly Notices of the ROYAL ASTRONOMICAL SOCIETY
MNRAS **513,** 2369–2384 (2022) https://doi.org/10.1093/mnras/stac890

Linking the properties of accreting white dwarfs with the ionization state of their ambient medium

D. Souropanis [1,2,3★] A. Chiotellis [1★] P. Boumis [1]
M. Chatzikos [4] S. Akras [1] L. Piersanti [5,6] A. J. Ruiter [7] and G. J. Ferland [4]

[1] *Institute for Astronomy, Astrophysics, Space Applications and Remote Sensing, National Observatory of Athens, 15236 Penteli, Greece*
[2] *Department of Physics, National and Kapodistrian University of Athens, Panepistimiopolis, 15784 Zografos, Greece*
[3] *Isaac Newton Group of Telescopes, Apartado 321, E-38700 Santa Cruz de La Palma, Canary Islands, Spain*
[4] *Department of Physics, University of Kentucky, Lexington, KY 40506, USA*
[5] *INAF – Osservatorio Astronomico d'Abruzzo, Via Mentore Maggini snc, I-64100 Teramo, Italy*
[6] *INFN – Sezione di Perugia, Via A. Pascoli snc, I-06123 Perugia, Italy*
[7] *School of Science, University of New South Wales, Australian Defence Force Academy, Canberra, ACT 2600, Australia*

Accepted 2022 March 24. Received 2022 March 24; in original form 2021 May 24

ABSTRACT

Steadily accreting white dwarfs (WDs) are efficient sources of ionization and thus are able to create extended ionized nebulae in their vicinity. These nebulae represent ideal tools for the detection of accreting WDs, given that in most cases the source itself is faint. In this work, we combine radiation transfer simulations with known H- and He-accreting WD models, providing for the first time the ionization state and the emission-line spectra of the formed nebulae as a function of the WD mass, the accretion rate and the chemical composition of the accreted material. We find that the nebular optical line fluxes and radial extent vary strongly with the WD's accretion properties, peaking in systems with WD masses of 0.8–1.2 $M_{\odot}$. Projecting our results on so-called BPT diagnostic diagrams, we show that accreting WD nebulae possess characteristics distinct from those of H II-like regions, while they have line ratios similar to those in galactic low-ionization emission-line regions. Finally, we compare our results with the relevant constraints imposed by the lack of ionized nebulae in the vicinity of supersoft X-ray sources (SSSs) and Type Ia supernova remnants – sources that are related to steadily accreting WDs. The large discrepancies uncovered by our comparison rule out any steadily accreting WD as a potential progenitor of the studied remnants and additionally require the ambient medium around the SSSs to be less dense than 0.2 cm^{-3}. We discuss possible alternatives that could bridge the incompatibility between the theoretical expectations and relevant observations.

Key words: line: formation – radiation mechanisms: general – binaries: general – white dwarfs – ISM: supernova remnants.

1 INTRODUCTION

White dwarfs (WDs) are the compact degenerate remnants of low- and intermediate-mass stars ($\sim$ 1–8 $M_{\odot}$), representing the endpoints of stellar evolution for the vast majority of stars in the Universe. Nuclear reactions having ceased in their centre, isolated WDs are doomed to quiescently fade out by radiating their internal energy. However, a high percentage of WDs are members of interacting binary systems (e.g. Toonen et al. 2017; Holberg 2009). In these systems, hydrogen- or helium-rich material can be transferred from the companion star to the WD, altering entirely its properties and expected evolution. Depending on the accretion process, the chemical composition of the accreting material, the WD mass and the nature of the companion star, these binary systems can reveal intriguing phenomena, and to date they have been linked to a number of astrophysical objects such as classical, recurrent and He novae (e.g. Gallagher & Starrfield 1978; Kato et al. 2000; Kemp et al. 2021), supersoft X-ray sources (van den Heuvel et al. 1992; Nomoto et al. 2007), symbiotic binaries (e.g. Mikołajewska 2007; Mohamed & Podsiadlowski 2012; Akras et al. 2019) and AM Canum Venaticorum (CVn) systems (e.g. Paczyński 1967; Nelemans et al. 2001; Piersanti, Yungelson & Tornambé 2015).

Carbon–oxygen WDs (CO WDs) in interacting binaries have also been proposed to be the progenitors of the cosmic explosions known as thermonuclear or Type Ia Supernovae (SNe Ia). It has been suggested that the explosion of the WD results either from mass accretion from a non-degenerate companion star (*single-degenerate scenario*; Whelan & Iben 1973) or from a merger with another WD (*double-degenerate scenario*; Iben & Tutukov 1984). While each scenario may produce an explosion through one or more explosion mechanisms, it is not clear so far which explosion mechanism is responsible (or dominant) in producing SNe Ia (see Ruiter 2020, for a recent review). In the Chandrasekhar-mass scenario, the required central density capable of initiating carbon ignition is reached when the WD approaches the Chandrasekhar mass limit ($M_{\rm WD} \sim 1.38\,M_{\odot}$). In an alternative scenario, the double-detonation scenario, an initial detonation of a He layer on a sub-Chandrasekhar-mass WD triggers a shock wave that rapidly propagates inside the WD's interior and compresses the central carbon, facilitating the

★ E-mail: d.souropanis@noa.gr (DS); a.chiotellis@noa.gr (AC)

onset of explosive carbon burning (e.g. Livne 1990; Fink et al. 2010; Sim et al. 2010; Woosley & Kasen 2011; Hillebrandt et al. 2013). Simulations have shown that the physical conditions adequate for reproducing 'normal' SNe Ia via the double-detonation mechanism are very favourable for CO WDs in the mass range $\approx$ 0.9–1.0 $M_\odot$ (see Piro, Thompson & Kochanek 2014; Shen et al. 2018, for details).

Given that CO WDs are typically formed with lower masses (the mass distribution of single CO WDs is peaked at $M \sim 0.56\,M_\odot$; Madej, Należyty & Althaus 2004), this implies that – at least for the vast majority of SNe Ia progenitors – mass accretion is required in order for the WD to reach the mass required for the explosion. For such progenitors, it has been shown that if the accretion rate is of the order of $\sim$ a few $\times 10^{-7}\,M_\odot\,yr^{-1}$ or $\sim$ a few $\times 10^{-6}\,M_\odot\,yr^{-1}$ for WDs accreting H- or He-rich material, respectively, shell nuclear burning occurs steadily, and the WD will increase in mass (e.g. Cassisi, Iben & Tornambè 1998; Nomoto et al. 2007; Shen & Bildsten 2007; Wolf et al. 2013; Piersanti, Tornambé & Yungelson 2014). WDs in such an accretion mode are characterized by surface temperatures exceeding 10^5 K. This means that a significant flux of UV and soft X-ray thermal photons are expected to be radiated from the surface of the accreting WD. In turn, these photons will photoionize the ambient medium in the vicinity, forming extended ionized nebulae bright in the He II 4686 Å, [O III] 5007 Å, and [O I] 6300 Å emission lines (Rappaport et al. 1994b). These nebulae should persist long after ($t > 10^4$ yr; Woods et al. 2018; Kuuttila et al. 2019) the WD accretion phase has ceased, until the majority of the ionized gas has recombined. For higher WD masses ($> 1.1\,M_\odot$), the surface temperature can reach up to a few $\times 10^6$ K, and hence the WD's photosphere becomes bright in the soft X-ray band (0.3–0.7 keV; van den Heuvel et al. 1992; Rappaport, Di Stefano & Smith 1994a). In fact, several permanent supersoft X-ray sources (SSSs) have been identified, and for many of them the optical and X-ray follow-up observations revealed that they are binary systems containing a WD that steadily burns the accreted material transferred by its companion star (van den Heuvel et al. 1992; Rappaport et al. 1994a; Kahabka & van den Heuvel 1997). Given that SSSs consist of a massive steadily accreting WD, these systems have been proposed as a potential prominent scenario for SNe Ia progenitors (Hachisu et al. 1999; Li & van den Heuvel 1997).

If indeed the WDs in progenitors of SNe Ia have passed through a steady accretion phase prior to their final explosion, then SNe Ia and their young remnants ($t_{SNR} \leq 10^4$ yr; hereafter SNRs Ia) should be surrounded by extended optically bright nebulae. Based on this fact, several independent studies were conducted in parallel, aiming to observe ionized nebulae around individual nearby SNe Ia (Graur & Woods 2019) and young SNRs Ia (e.g. Kuuttila et al. 2019; Farias et al. 2020). However, none of them detected any nebular optical emission around the studied objects, and thus strict limits were placed on the ionizing flux of their WD progenitors. An additional constraint on the ionizing flux of the SN Ia progenitors results from the presence of the Balmer-dominated shocks that most SNRs Ia display. Given that the Balmer lines indicate that the SNR is evolving into a – at least partially – neutral ambient medium, hot luminous WD progenitors seem incapable of explaining the properties of the vast majority of SNRs Ia (Woods et al. 2017, 2018).

Even more surprising is that, with the exception of CAL 83, ionized emission nebulae have not been detected around other SSSs (Remillard, Rappaport & Macri 1995; Farias et al. 2020). The lack of any nebular optical emission around the studied SSSs has been attributed either to a very low-density ambient medium or to an extremely transient SSS phase (Rappaport et al. 1994b; Woods & Gilfanov 2016; Farias et al. 2020). However, to date there is little understanding of the evolution of these systems and of the properties of the surrounding interstellar medium. Regarding the observed nebula around CAL 83, its origin remains under debate, as current models have difficulties in reproducing its optical emission-line ratios (Gruyters et al. 2012). A better understanding of the processes that govern the interaction of accreting WDs with their surrounding gas is an important task, given that in most cases the source itself is heavily obscured (Chen et al. 2015).

Past attempts at modelling the ionization state around accreting WDs focused on the class of SSSs. Thereby, these models were limited to the most massive and hottest members of the accreting WD family. In addition, for the description of the ionizing source, random pairs of luminosities and effective temperatures were adopted within the expected range that accreting WDs display (Rappaport et al. 1994b). However, detailed models of of stable nuclear burning on accreting WDs show that the WD's luminosity and effective temperature are strongly correlated with each other, and in turn strongly depend on the WD mass and mass accretion rate (e.g. Nomoto et al. 2007; Piersanti et al. 2014).

With the aim of further investigating the interaction of accreting WDs with their ambient medium and extending models from previous works, in this paper we link the properties of H- and He-accreting WDs with those of the surrounding ionized nebulae by coupling known WD accretion models from the literature with photoionization numerical tools. We explore the whole parameter space of steadily accreting WDs and present luminosities and surface-brightness profiles of various important nebular emission lines formed around these sources. In addition, we extend our study to the case of He-accreting WDs, systems that have not been studied in the past. In this way, we provide observational predictions for various nebular emission lines as a function of the WD mass, the accretion rate, and the chemical composition of the accreted material. In the second part of this paper, we compare our results with the observational constraints that exist as the result of the lack of ionized nebulae found around SSSs and SNRs Ia, (re-)assessing the plausibility of steadily nuclear-burning WDs as plausible progenitors for these objects.

This paper is organized as follows. In Section 2 we describe our radiation transfer simulations and present the results of our modelling regarding the ionization state and the spectral properties of ionized nebulae around steadily accreting WDs. In Section 3 we compare the results of our modelling with relevant observations from SSSs and SNRs Ia. We discuss and summarize our main results and conclusions in Sections 4 and 5.

2 MODELLING THE IONIZED NEBULAE AROUND STEADILY ACCRETING WHITE DWARFS

2.1 Methodology

To model the interaction of accreting WDs with their ambient medium, we use the photoionization code CLOUDY (v17.02, Ferland et al. 2017). CLOUDY is an open-source spectral synthesis code designed to simulate conditions in interstellar matter under a broad range of conditions (i.e. gas density, composition, incident spectrum, etc). More details, source files, and all necessary data are available from www.nublado.org.

To link the WD's mass accretion properties to those of the ionized ambient medium, we use the results produced from the accreting WD models of Nomoto et al. (2007) and Piersanti et al. (2014). Nomoto et al. (2007) studied the properties of CO WDs accreting

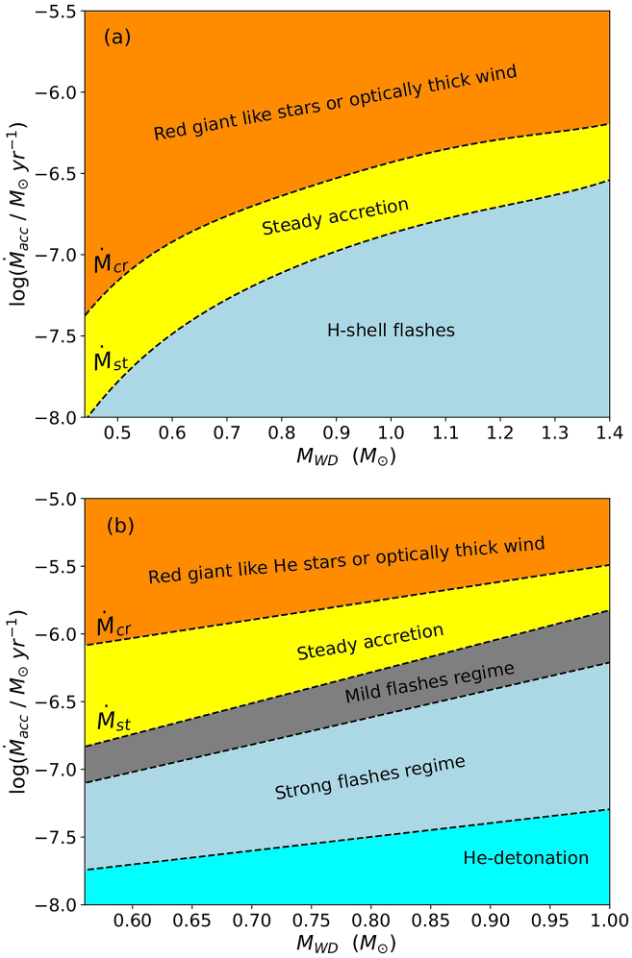

Figure 1. The possible accretion regimes for WDs accreting (a) H and (b) He, extracted by the models of Nomoto et al. (2007) and Piersanti et al. (2014), respectively. The dashed lines represent the borders between the regimes.

H-rich material in and near the steady accretion regime and they constructed steady models for various accretion rates and WD masses ranging from 0.5 to 1.38 $M_\odot$. Piersanti et al. (2014) studied the long-term evolution of He-accreting CO WDs for initial WD masses and accretion rates in the ranges 0.60–1.02 $M_\odot$ and 10^{-9}–10^{-5} $M_\odot yr^{-1}$, respectively. We refer to Nomoto et al. (2007) and Piersanti et al. (2014) for the full details of their models, while Fig. 1 shows the possible accretion regimes as a function of the WD mass (M_{WD}) and the accretion rate ($\dot{M}_{acc}$), as extracted from their models for H- and He-accreting WDs, respectively.

The steady accretion regime – the regime explored in this study – is confined in a narrow strip between the so-called stable and critical accretion rates ($\dot{M}_{st}$ and $\dot{M}_{cr}$). In this regime, the mass transfer is conservative, as the rate at which H/He is converted via surface nuclear burning into a He/CO mixture is equal or at least fairly close to the accretion rate. Consequently, the WD's intrinsic luminosity (L_{WD}) and its effective temperature (T_{eff}) are strongly paired with each other and dominantly determined from the mass-accretion rate and the WD mass. The results extracted by the aforementioned accreting WD models, namely the pairs of values for the WD's intrinsic luminosity and effective temperature as a function of the WD mass and accretion rate, are used as input parameters for the ionizing source in CLOUDY (see Appendix A). The central source is assumed to be a blackbody, which provides a reasonable approximation of the ionizing emission of nuclear-burning WDs, except far into the Wien tail (Chen et al. 2015; Woods et al. 2017). We further assume a spherical symmetry in our models, a constant-density ambient medium, and solar gas abundances (see the default solar values as defined in CLOUDY, which are taken from Grevesse & Sauval 1998; Allende Prieto, Lambert & Asplund 2001; Holweger 2001). The ambient medium number densities in our models are taken to be 0.2 cm^{-3} and 2 cm^{-3}, which are plausible values to use in the vicinity of SSSs (e.g. Farias et al. 2020) and of young SNRs Ia (e.g. Yamaguchi et al. 2014; Martínez-Rodríguez et al. 2018). We terminate our calculations when the gas temperature drops below 3000 K (at these low nebular temperatures, the hydrogen ionization fraction falls below 10 per cent, and thus its contribution to the total nebular line emission is negligible).

Given these assumptions, we estimate the predicted surface-brightness profile and luminosity in any emission line produced by the surrounding gas, for any given pair of WD mass and accretion rate within the stable accretion regime. In particular, CLOUDY provides the volume emissivity $e(r)$ of any emission line as a function of the distance r from the ionizing source. The surface brightness in a nebular spectral line, denoted by i, depends on the line-of-sight integral of the emission coefficient, which is given by

$$SB_i(r) = \int_s \frac{\epsilon_i(r)}{4\pi}\,\mathrm{d}s, \tag{1}$$

where the integral is taken along the line of sight through the nebula at impact parameter r from the centre of the nebula. The predicted total line luminosity is given by integrating the surface brightness over the area of the nebula, which is equivalent to integrating the emission coefficient over the volume of the ionized nebula, which is given by

$$L_i = \int_0^r SB_i(r) 2\pi r\,\mathrm{d}r. \tag{2}$$

2.2 Results

In order to offer direct links between the properties of H- and He-accreting WDs and those of their ambient medium, we present in Tables 1 and 2, respectively, the luminosities of the most important optical diagnostic nebular emission lines as a function of WD accretion properties (i.e. the WD's mass, accretion rate, intrinsic luminosity and effective temperature) and for the two studied interstellar medium (ISM) densities (n_{ism} = 0.2 and 2 cm^{-3}). As an index for the ionizing efficiency of steadily accreting, nuclear-burning WDs, for each combination of WD mass and accretion rate we also provide the parameters $R_{H^0,\,0.5}$ and $R_{He^0,\,0.5}$ (fifth and sixth columns of Tables 1 and 2), which indicate the radial distance from the central source at which the neutral H and He are equal to the corresponding ionized component(s), namely 50 per cent each. Given the large parameter space involved in the results tabulated in Tables 1 and 2, the variability of the nebular emission lines' luminosity and the radial extent of the regions of ionized H and ionized He as a function of the studied physical variables cannot be firmly drawn. However, the following distinctive patterns can be discerned.

(i) On average, the brightest and most prominent optical emission lines of the ionized nebulae of the studied H/He nuclear-burning WD

Table 1. Predicted nebular radii and luminosities of prominent optical emission lines surrounding H-accreting WDs as a function of WD mass for the two stability boundaries of accretion rate in the steady accretion regime, based on the models of Nomoto et al. (2007), and an ISM with a constant density of 0.2 or 2 cm^{-3}.

						H-accreting WDs								
M	$\dot{M}_{\rm acc}$	$\log(L/{\rm L}_\odot)$	$\log(T_{\rm eff}/{\rm K})$	$R_{\rm H^0,0.5}$	$R_{\rm He^0,0.5}$	He II	[O III]	[O I]	[O II]	Hα	Hβ	[N II]	[N II]	[S II]
	($\times$ 10^{-7}					4686 Å	5007 Å	6300 Å	3727 Å	6562 Å	4861 Å	5754 Å	6584 Å	6717 Å
(M$_\odot$)	M$_\odot$ yr^{-1})			(pc)	(pc)	(erg s^{-1})	(erg s^{-1})	(erg s^{-1})	(erg s^{-1})	(erg s^{-1})	(erg s^{-1})	(erg s^{-1})	(erg s^{-1})	(erg s^{-1})
						$n_{\rm ism}$ = 2 cm^{-3}								
0.6	0.3258	3.38	5.39	9.72	11.7	2.03e + 34	2.72e + 35	4.28e + 34	4.72e + 35	1.45e + 35	5.15e + 34	2.76e + 33	1.85e + 35	1.69e + 35
0.6	1.2	3.95	4.87	16.3	17.3	7.26e + 33	5.92e + 35	3.29e + 34	7.10e + 35	9.27e + 35	3.30e + 35	2.73e + 33	3.85e + 35	2.89e + 35
0.8	0.775	3.76	5.57	11.3	14.3	3.85e + 34	4.83e + 35	1.17e + 35	9.69e + 35	2.62e + 35	9.18e + 34	6.17e + 33	3.69e + 35	2.93e + 35
0.8	2.3	4.23	5.44	18.4	21.2	1.59e + 35	2.78e + 36	2.61e + 35	3.17e + 36	1.01e + 36	3.57e + 35	1.94e + 34	1.16e + 36	9.77e + 35
1.0	1.35	4.00	5.72	11.7	15.8	4.51e + 34	5.19e + 35	2.06e + 35	1.30e + 36	3.49e + 35	1.20e + 35	8.71e + 33	5.00e + 35	3.06e + 35
1.0	3.7	4.45	5.54	20	24.2	2.24e + 35	3.75e + 36	5.22e + 35	4.88e + 36	1.41e + 36	4.94e + 35	3.14e + 34	1.77e + 36	1.28e + 36
1.25	2.15	4.20	5.91	10.6	15.5	3.56e + 34	3.48e + 35	2.70e + 35	1.25e + 36	3.62e + 35	1.22e + 35	8.85e + 33	5.10e + 35	2.43e + 35
1.25	5.4	4.64	5.67	21.1	26.9	2.71e + 35	4.39e + 36	9.08e + 35	6.70e + 36	1.86e + 36	6.40e + 35	4.49e + 34	2.44e + 36	1.40e + 36
1.35	2.55	4.28	6.03	9.3	13.9	2.37e + 34	2.04e + 35	2.44e + 35	9.47e + 35	3.03e + 35	1.01e + 35	7.08e + 33	4.22e + 35	1.87e + 35
1.35	6	4.70	5.81	18.8	25.6	1.98e + 35	2.84e + 36	1.08e + 36	6.10e + 36	1.66e + 36	5.61e + 35	4.19e + 34	2.29e + 36	1.03e + 36
1.38	2.75	4.31	6.10	8.5	12.7	1.82e + 34	1.46e + 35	2.17e + 35	7.75e + 35	2.64e + 35	8.79e + 34	5.96e + 33	3.62e + 35	1.60e + 35
1.38	6.2	4.71	5.87	17.5	24.6	1.61e + 35	2.17e + 36	1.05e + 36	5.28e + 36	1.50e + 36	5.03e + 35	3.75e + 34	2.08e + 36	8.81e + 35
						$n_{\rm ism}$ = 0.2 cm^{-3}								
0.6	0.3258	3.38	5.39	43	57.4	1.58e + 34	1.25e + 35	4.96e + 34	4.05e + 35	1.33e + 35	4.72e + 34	2.34e + 33	1.79e + 35	1.83e + 35
0.6	1.2	3.95	4.87	76	83.1	7.06e + 33	3.28e + 35	3.68e + 34	6.17e + 35	9.27e + 35	3.28e + 35	2.22e + 33	4.05e + 35	3.36e + 35
0.8	0.775	3.76	5.57	49.3	67.9	2.91e + 34	2.10e + 35	1.18e + 35	7.94e + 35	2.26e + 35	7.92e + 34	4.95e + 33	3.33e + 35	3.12e + 35
0.8	2.3	4.23	5.44	82.3	103.4	1.31e + 35	1.52e + 36	3.32e + 35	3.17e + 36	9.29e + 35	3.29e + 35	1.90e + 34	1.27e + 36	1.17e + 36
1.0	1.35	4.00	5.72	49.9	71.6	3.29e + 34	2.10e + 35	1.75e + 35	9.77e + 35	2.79e + 35	9.66e + 34	6.38e + 33	4.07e + 35	3.17e + 35
1.0	3.7	4.45	5.54	88.9	114.8	1.79e + 35	1.95e + 36	5.81e + 35	4.63e + 36	1.26e + 36	4.41e + 35	2.92e + 34	1.81e + 36	1.52e + 36
1.25	2.15	4.20	5.91	43.3	67	2.41e + 34	1.24e + 35	1.86e + 35	8.07e + 35	2.55e + 35	8.69e + 34	5.56e + 33	3.51e + 35	2.19e + 35
1.25	5.4	4.64	5.67	91.9	124.8	2.11e + 35	2.16e + 36	8.87e + 35	5.95e + 36	1.59e + 36	5.51e + 35	3.88e + 34	2.32e + 36	1.65e + 36
1.35	2.55	4.28	6.03	36.7	57.9	1.51e + 34	6.59e + 34	1.48e + 35	5.54e + 35	1.92e + 35	6.50e + 34	3.98e + 33	2.55e + 35	1.46e + 35
1.35	6	4.70	5.81	80	115	1.46e + 35	1.24e + 36	8.81e + 35	4.65e + 36	1.31e + 36	4.47e + 35	3.16e + 34	1.88e + 36	1.11e + 36
1.38	2.75	4.31	6.10	33.5	53.1	1.12e + 34	4.51e + 34	1.23e + 35	4.29e + 35	1.56e + 35	5.26e + 34	3.17e + 33	2.06e + 35	1.15e + 35
1.38	6.2	4.71	5.87	73.7	107.4	1.16e + 35	8.93e + 35	8.04e + 35	3.87e + 36	1.13e + 36	3.83e + 35	2.67e + 34	1.60e + 36	8.89e + 35

Table 2. Predicted nebular radii and luminosities of prominent optical emission lines surrounding He-accreting WDs as a function of WD mass for the two stability boundaries of accretion rate in the steady accretion regime, based on the models of Piersanti et al. (2014), and an ISM with a constant density of 0.2 or 2 cm^{-3}.

						He-accreting WDs								
M ($M_\odot$)	$\dot{M}_{acc}$ ($\times$ 10^{-6} $M_\odot$ yr^{-1})	$\log(L/L_\odot)$	$\log(T_{eff}/K)$	$R_{H^0,0.5}$ (pc)	$R_{He^0,0.5}$ (pc)	He II 4686 Å (erg s^{-1})	[O III] 5007 Å (erg s^{-1})	[O I] 6300 Å (erg s^{-1})	[O II] 3727 Å (erg s^{-1})	Hα 6562 Å (erg s^{-1})	Hβ 4861 Å (erg s^{-1})	[N II] 5754 Å (erg s^{-1})	[N II] 6584 Å (erg s^{-1})	[S II] 6717 Å (erg s^{-1})
						$n_{ism} = 2$ cm^{-3}								
0.6	0.15	3.33	5.28	9.9	11.5	1.83e + 34	2.77e + 35	3.21e + 34	4.14e + 35	1.52e + 35	5.42e + 34	2.31e + 33	1.70e + 35	1.52e + 35
0.6	0.95	4.03	4.78	16.7	17.3	2.37e + 33	3.85e + 35	1.82e + 34	5.15e + 35	1.10e + 36	3.89e + 35	1.65e + 33	3.29e + 35	2.34e + 35
0.7	0.3	3.73	5.43	12.4	14.9	4.70e + 34	6.92e + 35	9.44e + 34	1.04e + 36	3.13e + 35	1.11e + 35	6.29e + 33	3.97e + 35	3.49e + 35
0.7	1.80	4.34	4.80	21.4	22.2	7.28e + 33	1.13e + 36	4.52e + 34	1.25e + 36	2.25e + 36	7.98e + 35	4.34e + 33	7.11e + 35	4.99e + 35
0.8	0.52	4.03	5.56	14.3	17.8	7.91e + 34	1.13e + 36	2.14e + 35	1.88e + 36	5.20e + 35	1.82e + 35	1.20e + 34	7.01e + 35	5.41e + 35
0.8	1.90	4.49	5.05	25.6	27.1	1.45e + 35	5.62e + 36	2.10e + 35	4.29e + 36	2.96e + 36	1.06e + 36	2.12e + 34	1.79e + 36	1.39e + 36
0.9	0.71	4.26	5.69	15.1	19.9	9.73e + 34	1.34e + 36	3.84e + 35	2.65e + 36	7.10e + 35	2.45e + 35	1.77e + 34	9.93e + 35	6.01e + 35
0.9	2.70	4.63	5.25	27.6	29.4	4.10e + 35	9.93e + 36	3.54e + 35	7.00e + 36	3.30e + 36	1.19e + 36	3.92e + 34	2.61e + 36	2.12e + 36
1.0	1.40	4.40	5.77	15.3	20.8	1.04e + 35	1.37e + 36	5.26e + 35	3.10e + 36	8.45e + 35	2.88e + 35	2.13e + 34	1.18e + 36	6.07e + 35
1.0	2.90	4.71	5.44	27	30.1	5.21e + 35	1.04e + 37	6.74e + 35	9.34e + 36	3.14e + 36	1.11e + 36	5.58e + 34	3.19e + 36	2.59e + 36
						$n_{ism} = 0.2$ cm^{-3}								
0.6	0.15	3.33	5.28	44.4	56.9	1.46e + 34	1.36e + 35	3.98e + 34	3.73e + 35	1.43e + 35	5.13e + 34	2.03e + 33	1.72e + 35	1.71e + 35
0.6	0.95	4.03	4.78	77.8	81.9	2.33e + 33	2.08e + 35	1.99e + 34	4.17e + 35	1.10e + 36	3.88e + 35	1.25e + 33	3.31e + 35	2.65e + 35
0.7	0.3	3.73	5.43	55.6	72.6	3.71e + 34	3.36e + 35	1.12e + 35	9.46e + 35	2.86e + 35	1.014e + 35	5.61e + 33	3.99e + 35	3.91e + 35
0.7	1.80	4.34	4.80	99.6	105.3	7.23e + 33	6.41e + 35	5.15e + 34	1.10e + 36	2.25e + 36	7.96e + 35	3.59e + 33	7.69e + 35	5.96e + 35
0.8	0.52	4.03	5.56	62.6	84.5	6.14e + 34	5.33e + 35	2.25e + 35	1.65e + 36	4.55e + 35	1.60e + 35	1.03e + 34	6.70e + 35	6.03e + 35
0.8	1.90	4.49	5.05	118.6	131.7	1.40e + 35	3.66e + 36	2.83e + 35	4.54e + 36	2.94e + 36	1.05e + 36	2.16e + 34	2.14e + 36	1.78e + 36
0.9	0.71	4.26	5.69	64.9	91.7	7.41e + 34	5.93e + 35	3.51e + 35	2.15e + 36	5.90e + 35	2.05e + 35	1.40e + 34	8.71e + 35	6.61e + 35
0.9	2.70	4.63	5.25	127.1	143.36	3.71e + 35	6.65e + 36	5.41e + 35	8.01e + 36	3.23e + 36	1.16e + 36	4.41e + 34	3.27e + 36	2.82e + 36
1.0	1.40	4.40	5.77	65.2	92.9	7.69e + 34	5.78e + 35	4.37e + 35	2.38e + 36	6.68e + 35	2.30e + 35	1.59e + 34	9.70e + 35	6.44e + 35
1.0	2.90	4.71	5.44	121	145.5	4.41e + 35	6.34e + 36	9.20e + 35	9.88e + 36	2.94e + 36	1.04e + 36	5.98e + 34	3.78e + 36	3.31e + 36

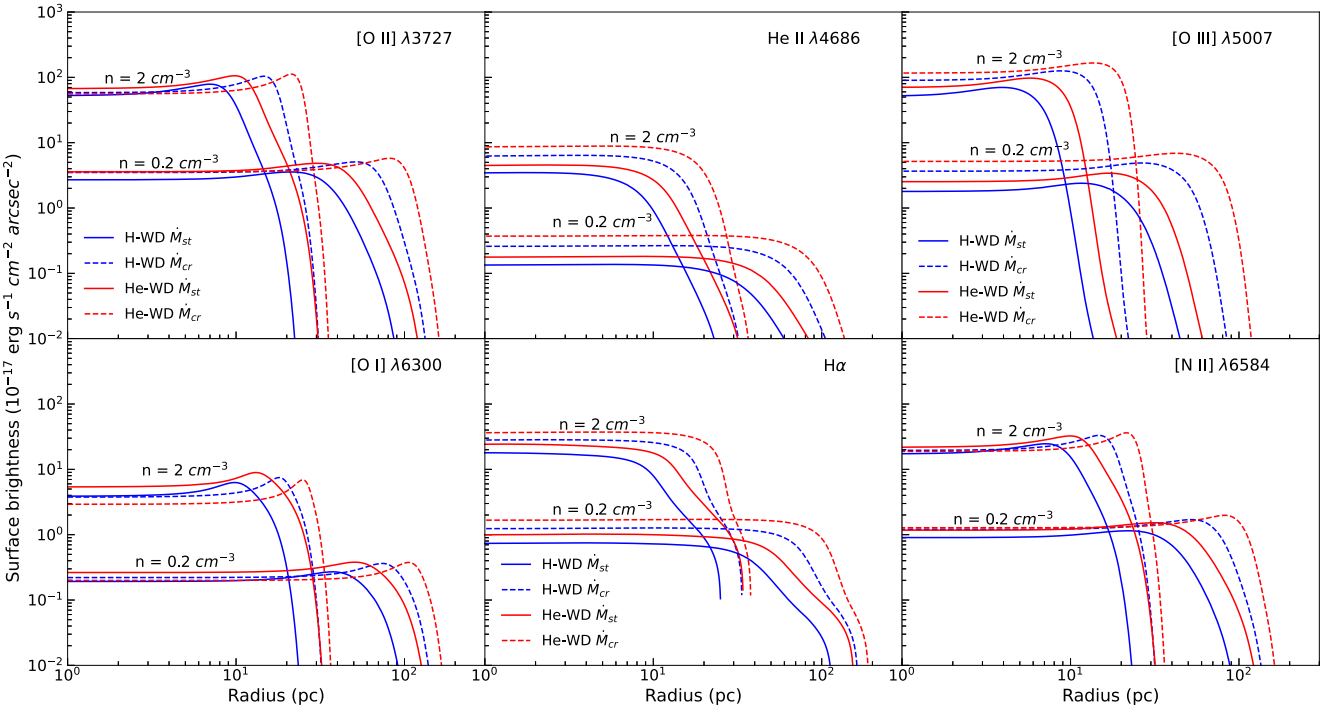

Figure 2. Comparison of surface-brightness profiles for six prominent optical emission lines of nebulae ionized by a 1 $M_\odot$ WD accreting H- and He-rich matter at the two corresponding limits of the accretion rate in the steady accretion regime ($\dot{M}_{\rm st}$ and $\dot{M}_{\rm cr}$). In each panel, the surface-brightness profiles are shown for two constant ISM densities, 0.2 and 2 cm^{-3}.

models – in descending order – are: [O II] 3727 Å,[1] [O III] 5007 Å, Hα, [N II] 6584 Å and [S II] 6717 Å. Concerning the radial extent of the spheres of ionized H and He around accreting WDs, we find that the quantity $R_{\rm He^0,\ 0.5}$ is about 1.1–1.6 larger than the $R_{\rm H^0,\ 0.5}$ in all of our models at both tested densities.

(ii) The increase of the WD's accretion rate from its minimum value ($\dot{M}_{\rm st}$) to its maximum ($\dot{M}_{\rm cr}$) leads to a substantial enhancement for almost all line luminosities by about one order of magnitude. Exceptions to this trend are the lines of He II 4686 Å, [O I] 6300 Å and [N II] 5754 Å, for which the increase of the mass accretion rate is accompanied by a modest decrease of their luminosity for the case of low-mass H- and He-accreting WDs ($M_{\rm WD} \lesssim 0.8\,M_\odot$). The principal impact on the sizes of H and He ionized regions around accreting WDs is the formation of more extended nebulae, whose radii are predicted to increase by a factor of 2 when the accretion rate increases from its minimum value to its maximum one.

(iii) Apart from the accretion rate, the line luminosities are highly sensitive to the WD mass. The brightest and most extended ionized nebulae around H-accreting WDs are expected to accompany systems with WD masses ranging from 0.8 to 1.2 $M_\odot$, while in the case of He-accreting WDs, the relevant mass range is 0.8–1.0 $M_\odot$. This result is important in the context of SNe Ia progenitors, as sub-Chandrasekhar CO WDs accreting H/He-rich material are predicted to leave more conspicuous imprints in the form of ionized, optically bright nebulae, which are more likely to be detected than those resulting from H-accreting, Chandrasekhar-mass WDs.

(iv) Overall, the predicted line luminosities of the nebulae surrounding He-accreting WDs are higher than those surrounding H-accreting WDs. This is because He-accreting WDs tend to be more luminous and hotter sources, as the lower energy released per unit mass by He nuclear burning is counterbalanced by the higher accretion rates required for the He-accreting WD's steady accretion regime.

(v) Most of the nebular line luminosities show low sensitivity to the ambient medium density, decreasing or increasing only moderately (depending on the properties of the H/He-accreting WD) as the density increases from 0.2 to 2 cm^{-3}. A noticeable exception is the [O III] 5007 Å line, for which an increase by one order of magnitude in the surrounding ISM density results in a strong enhancement by two to three times in its line luminosity. Thus, accreting WDs embedded in denser environments produce brighter [O III] nebulae, where in some cases – for example for massive WDs accreting He-rich matter at high rates – the [O III] 5007 Å can be the dominant emission line. Finally, concerning the radial extent of the H and He ionized regions (as described by the parameters $R_{\rm H^0,\ 0.5}$ and $R_{\rm He^0,\ 0.5}$), the increase of the ISM density by one order of magnitude results in a decrease of the relevant radii by about a factor of 4.

In order to clarify how the observables of nuclear-burning WD nebulae depend on the accretion rate, the chemical composition of the accreted material and the ISM density, we compare in Fig. 2 the extracted surface-brightness profiles for six prominent optical emission lines of nebulae ionized by a 1 $M_\odot$ WD, accreting H/He-rich matter at the two corresponding limits of the steady accretion regime and for $n_{\rm ism} = 0.2$ and 2 cm^{-3}. Even if, as mentioned above, the line luminosities are not sensitive to the ambient medium density, the radial distribution of the nebular surface brightness changes substantially with the gas density. As expected, decreasing the ISM density results in a more extended, but fainter, ionized nebula formation. In addition, as illustrated in our plots, WDs with

[1]The line [O II] 3727 Å refers to the combined emission of [O II] 3726.03 Å and [O II] 3728.73 Å.

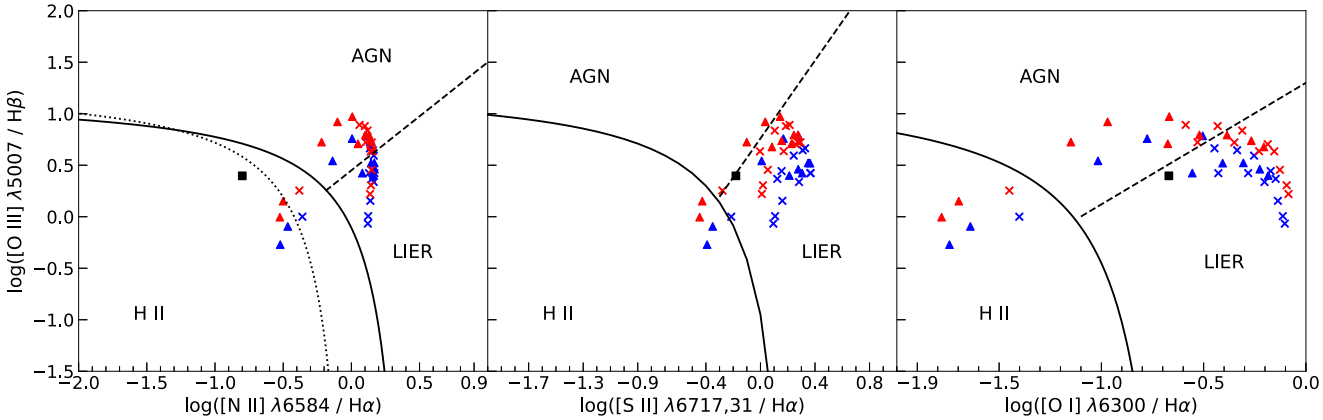

Figure 3. Diagnostic line-ratio diagrams for nebulae ionized by H-accreting (crosses) and He-accreting (triangles) WDs compared with H II regions, LIERs and AGN-like objects. The blue colour corresponds to the ambient medium density of $n_{\rm ism} = 0.2$ cm^{-3} and the red one to $n_{\rm ism} = 2$ cm^{-3}. Left: [O III]/Hβ versus [N II]/Hα nebular line ratios. The solid curve is the theoretically modelled 'extreme starburst line' (Kewley et al. 2001), the dotted line shows the Kauffmann et al. (2003) selection criteria, while the dashed line represent the AGN–LIER demarcation by Schawinski et al. (2007). Middle and right: [O III]/Hβ versus [S II]/Hα and [O III]/Hβ versus [O I]/Hα, respectively. The solid and the dashed lines in the middle and right diagrams represent the criteria of Kewley et al. (2006) used to separate H II regions, AGNs, and LIERs. For comparison, we plot the estimated line ratios from a subregion of the CAL 83 nebula (black square) as extracted by Gruyters et al. (2012).

higher accretion rates are expected to be surrounded by brighter and more extended ionized nebulae, and thus are more likely to be detected. The same applies for He-accreting WDs, as they are hotter and brighter sources than their H-accreting counterparts, and this has a direct impact on the size and the surface brightness of their surrounding ionized nebulae. Regarding the radial distribution of the surface brightness of each nebular line, the He II λ4686 and Hα lines reveal a rather flat curve, which after a given radius declines rapidly. By contrast, the surface brightnesses of the three oxygen forbidden lines ([O II] 3727 Å, [O III] 5007 Å and [O I] 6300 Å) and of the [N II] 6584 Å line initially increase moderately with increasing distance from the source until a local peak can be seen, after which they sharply decline. The radial positions of these peaks and the subsequent decrease of the surface brightness differ for each nebular line. Therefore, the nebular line ratios are expected to change substantially moving outwards from the ionizing source, and hence it is very important to consider the radial distance over which the line ratio has been obtained. Intriguingly, the succession of local maxima in the nebula's surface brightness as a function of the radial distance from the source is in the same order as the flux peaks observed in the CAL 83 nebula, with the [N II] and [O I] lines peaking further out than the [O III], Hα and He II lines. This result supports the idea that the observed nebula in the vicinity of CAL 83 is produced by the ionizing activity of the accreting WD.

Finally, we investigate the imprint of the nebulae around steadily accreting WDs as compared with those resulting from other ionizing sources, such as massive stars and accreting black holes, by projecting our results in the phase-space of the so-called 'BPT' diagrams (Baldwin, Phillips & Terlevich 1981). These diagrams use the [O III]/Hβ versus [N II]/Hα, [S II]/Hα and [O I]/Hα line ratios as an index that separates objects with different ionizing spectra. The line ratios of our models have been estimated by integrating the line luminosities over the entire nebula for solar gas abundances and for the two studied ISM densities (0.2 and 2 cm^{-3}). In the same plots, we also include the theoretically/empirically derived relationships that indicate the regimes of galactic low-ionization emission-line regions (LIERs), active galactic nuclei (AGNs) and H II region-like objects (see Fig. 3).

As Fig. 3 illustrates, the nebular flux ratios around H-accreting WDs in the lower ionization lines [N II], [S II] and [O I], relative to Hα, are much higher than the ionization by young massive stars (H II regions), while the [O III]/Hβ line ratio is overall lower compared with the gas ionized by AGN-like objects. One exception is the low-mass WD population with high accretion rates ($M_{\rm WD} \leq 0.6\,{\rm M}_{\odot}$); these coincide with the loci of H II regions. This result is due to the low photospheric temperatures ($T_{\rm eff} < 55000$ K) and luminosities ($\log(L/{\rm L}_{\odot}) < 3.5$) that characterize this subclass of H-accreting WDs and thus, they possess ionizing properties comparable to those of massive OB stars. On the other hand, for the high-ISM-density case ($n_{\rm ism} = 2\,{\rm cm}^{-3}$), the rapidly accreting WDs in the mass range of $M_{\rm WD} \sim 0.8$–$1.0\,{\rm M}_{\odot}$, owing to their high ionizing efficiency, produce enhanced [O III]/Hβ line ratios and overlap with the AGN region. However, apart from those exceptions, the vast majority of the nebulae around H-accreting WDs are well within the loci of LIERs.

The class of He-accreting WDs, being hotter and more luminous sources than their H-accreting counterparts, produce ionized nebulae characterized by higher [O III]/Hβ ratios. Consequently, more members of this class are found in the AGN regime. These are mainly the WDs with masses in the range of $M_{\rm WD} \sim 0.8$–$1.0\,{\rm M}_{\odot}$ that steadily accrete He at the maximum possible rate ($\dot{M}_{\rm acc} \sim \dot{M}_{\rm cr}$). Similar to the previous case, the rapidly He-accreting, low-mass WDs ($M_{\rm WD} \sim 0.6$–$0.8\,{\rm M}_{\odot}$) are found within the H II region. For the WDs that accrete He-rich material at low accretion rates, we find that there is not a great distinction from the H-accreting ones and they are also found in the general area of LIERs.

In the same diagrams we also plot the relevant observations of Gruyters et al. (2012), who provide a spectroscopic study of a subregion around CAL 83, the only known ionized nebula around a SSS. The observed flux ratio values [O III]/H$\beta = 2.50$, [S II]/H$\alpha = 0.65$ and [O I]/H$\alpha = 0.21$ of the nebula around CAL 83 coincide with the regions where our models are placed. This is not the case for the observed [N II]/H$\alpha = 0.15$ ratio, which is slightly lower than our model's predicted range. This discrepancy can be explained by the fact that CAL 83 is in the Large Magellanic Cloud, where the metallicities are probably smaller by factor of 2–8, as well as by the fact that these line ratios arise from about one-quarter of the

Table 3. Properties of SNRs Ia considered in this study and constraints on their ambient medium. SNR parameters: column 1, the name of each SNR; columns 2 and 3, the present radius in parsecs and age in years of each SNR; column 4, logarithm of the luminosity's upper limit (erg s^{-1}) enclosed within 6.8 pc of the central source; column 5, upper limits on the He II 4686 Å surface brightness for each SNR; column 6, the minimum required neutral hydrogen fraction at the present radius of the shock of each SNR; column 7, the pre-shock gas density range of each SNR as presented in the current literature. References: (1) Rest et al. (2005); (2) Kosenko, Ferrand & Decourchelle (2014); (3) Farias et al. (2020); (4) Kuuttila et al. (2019); (5) Warren & Hughes (2004); (6) Ghavamian et al. (2002); (7) Ghavamian et al. (2003); (8) Ghavamian et al. (2001); (9) Ghavamian et al. (2007); (10) Lewis et al. (2003); (11) Yamaguchi et al. (2014); (12) Badenes et al. (2006); (13) Tian & Leahy (2011); (14) Kosenko et al. (2008); (15) Williams et al. (2014); (16) Raymond et al. (2007); (17) Seitenzahl et al. (2019); (18) Rakowski, Ghavamian & Hughes (2003); (19) Acero, Ballet & Decourchelle (2007); (20) Williams et al. (2013); (21) Katsuda et al. (2010).

SNRs	Radius (pc)	Age (yr)	$\log(L_{\rm O\,III,\,6.8\,pc})$ (erg s^{-1})	He II 4686 Å surface brightness ($\times 10^{-19}$ erg s^{-1} cm^{-2} $arcsec^{-2}$)	f_{H^0}	n_0 (cm^{-3})	References
0519-69.0	4 ± 0.3	600 ± 200	34.08	5.3	0.4–0.5	1–2	1, 2, 3, 4, 9, 17
0509-67.5	3.6	400 ± 120	33.75	4.2	>0.4	0.1–0.6	1, 2, 3, 4, 5, 9, 14, 17
N103B	3.6	860 ± 400	Unknown	5.7	Unknown	1–2.5	1, 4, 10, 15
DEM L71	6.8–9	∼4700	Unknown	4.7	0.2–0.4	0.5–1.5	4, 7, 9, 18
SN 1006	10	∼1000	Unknown	Unknown	>0.1	0.05–0.4	6, 11, 16, 19
Tycho	3.3 ± 0.3	∼434	Unknown	Unknown	>0.8	0.1–0.9	8, 12, 13, 20, 21

Table 4. Logarithmic upper limits of the [O III] 5007 Å luminosity (erg s^{-1}) enclosed within 6.8 pc of the central source for various SSSs, as extracted by the works of Remillard et al. (1995) and Farias et al. (2020). CAL 87 2 and CAL 87 3 refer to the observations of CAL 87 obtained at two different epochs.

SSSs	$\log(L_{\rm O\,III,\,6.8\,pc})$
RX J0550.0–7151	33.58
RX J0513.9–6951	34.20
CAL 87 2	34.01
CAL 87 3	34.14
Remillard + 95	34.22

inner region of the nebula, while our theoretical results concern the integrated luminosity of the entire nebula. As we have shown in this section, different regions of the nebula around accreting WDs possess different line ratios (see also Rappaport et al. 1994b; Remillard et al. 1995; Gruyters et al. 2012, for a similar argumentation). Further observations, covering the entire nebula of CAL 83, and a targeted modelling are required to provide a better understanding of the properties of the ionizing source and its surrounding gas.

3 COMPARISON WITH THE OBSERVABLES OF SUPERSOFT X-RAY SOURCES AND TYPE IA SNRS

Having determined the traces of accreting WDs on their surrounding gas, in this section we compare the results extracted by our modelling with the relevant constraints imposed by optical observations. In particular, we assess the compatibility of steadily accreting WDs with the constraints acquired by the lack of (relic) ionized nebulae around a number of SSSs and SNRs Ia (Rappaport et al. 1994b; Kuuttila et al. 2019; Farias et al. 2020) as well as by the existence of the Balmer-dominated shocks found in many SNRs Ia (Woods et al. 2017, 2018).

3.1 Upper limits of [O III] 5007 Å line luminosities enclosed within 6.8 pc of SSSs and SNRs Ia

The ionization state of the ambient medium around SSSs and SNRs Ia is well constrained by optical observations in the [O III] λ5007 line, which is expected to be one of the dominant emission lines in the ionized nebulae around accreting WDs (see Section 2.2). The recombination time-scale for doubly ionized oxygen responsible for the forbidden line [O III] λ5007 is $\sim 10^4 (n_{\rm ism}/1{\rm cm}^{-3})^{-1}$yr (Osterbrock & Ferland 2006), so for any hot, luminous progenitor scenario, young SNRs would still be surrounded by these associated nebulae long after the explosion.

Remillard et al. (1995) searched for [O III]-bright nebulae around 10 SSSs[2] in the Small and Large Magellanic Clouds (SMC and LMC, respectively). They did not detect any optical emission around these sources except for one case, CAL 83. For the remaining SSSs, they set an upper limit of $10^{34.22}$ erg s^{-1} on their [O III] line luminosities enclosed within 6.8 pc of the central sources.[3]

Later, Farias et al. (2020), aiming to revisit some of the fields studied by Remillard et al. (1995), used advanced modern instruments and searched for nebulae around four of the studied LMC SSSs (CAL 83, CAL 87, RX J0550.0–7151 and RX J0513.9–6951). In addition, they extended their work to SNRs Ia, where they searched for relic nebulae in the vicinity of three young LMC SNRs Ia: N103B, SNR 0519–69.0 and SNR 0509–67.5. The authors confirmed that no [O III] ionized regions were detected around the studied SSSs and SNRs Ia,[4] except for the SSS CAL 83, thus establishing more sensitive upper limits on the [O III] nebular line luminosities. In Tables 3 (fourth column) and 4, the upper limits are summarized for the [O III] 5007 Å luminosity enclosed within 6.8 pc of the central source for the SNRs and the SSSs, as extracted by the works of Remillard et al. (1995) and Farias et al. (2020).

In order to provide a direct comparison of our theoretical predictions with the upper limits acquired from the observations, we follow the same methodological approach as described in Section 2.1 and calculate the nebular [O III] line luminosity enclosed at 6.8 pc around H- and He-nuclear-burning WDs. This time in our modelling we assume a LMC-like chemical gas composition because the majority of our sample is in the LMC, with abundances one-half of the solar

[2]The LMC targets in their study were CAL 83, CAL 87, RXJ 0439.8-6809, RXJ 0513.9–6951, RXJ 0527.8–6954 and RX J0550.0–7151, while the SMC targets were 1E 0035.4–7230, RXJ O048.4–7332, 1E 0056.8–7154 and RXJ 0058.6–7146.

[3]7.5 pc in their work, but they have assumed an LMC distance of 55 kpc.

[4]The only exception was SNR N103B, for which they detected some emission, but they concluded that this emission does not correspond to a diffuse [O III] ionized nebula around the source.

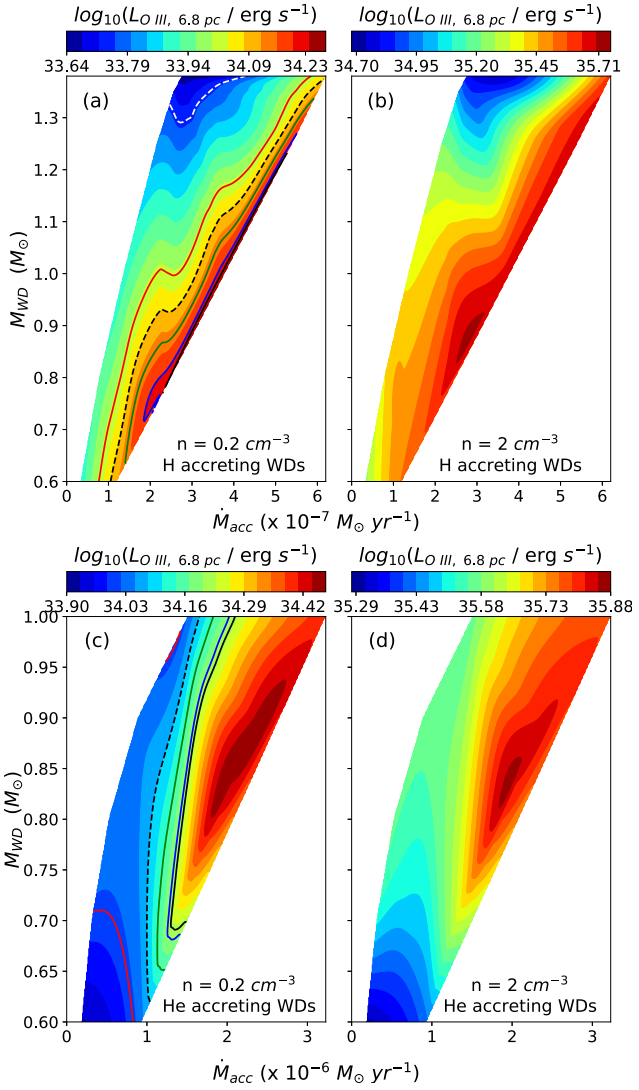

Figure 4. The [O III] 5007 Å luminosity enclosed within 6.8 pc radius as a function of the accretion rate and the WD mass in the steady accretion regime for (a) H-accreting WDs and constant ISM density 0.2 cm^{-3}, (b) H-accreting WDs and constant ISM density 2 cm^{-3}, (c) He-accreting WDs and constant ISM density 0.2 cm^{-3}, and (d) He-accreting WDs and constant ISM density 2 cm^{-3}. The black solid line represents the upper limits for the SSSs established by Remillard+95 while the blue, green and red solid lines represent the upper limits acquired for RX J0513.9–6951, CAL 87 3 and CAL 87 2, respectively.

values (Choudhury et al. 2018). The ambient medium number density in our models is taken to be 0.2 cm^{-3} and 2 cm^{-3}, values that can be considered as conservative lower and upper bounds for the bulk ambient medium properties found around SSSs (e.g. Farias et al. 2020) and of young SNRs Ia (e.g. Yamaguchi et al. 2014; Martínez-Rodríguez et al. 2018), and that are in line with the independent estimates of the pre-shocked densities of the remnants involved in this study (Table 3, seventh column).

In Fig. 4 we plot the upper limits of the [O III] luminosity extracted by observations, together with the luminosity predicted by our models as a function of the WD mass and accretion rate, for the two studied ISM densities. Our results clearly illustrate that the assumed ISM density around the SSSs and SNRs substantially alters the constraints imposed by observations in terms of the accreting WD properties. Specifically, for a gas density equal to 2 cm^{-3}, all of our models lie well above the derived upper limits for all the SSSs and SNRs Ia of our sample (see Figs 4b, d). This means that if the density of the ambient medium around these objects is close to or higher than 2 cm^{-3}, none of the nuclear-burning WD models is able to reproduce the relevant observables.

By contrast, when the density drops from 2 to 0.2 cm^{-3}, we find that within our studied parameter space not all accreting WD models are excluded (Figs 4a,c). Specifically, we cannot rule out any sub-Chandrasekhar or Chandrasekhar-mass WD accreting H/He-rich matter with low or intermediate accretion rates in the steady accretion regime for SNR 0519–69.0. Stricter constraints are placed for the progenitors of SNR 0509–67.5, where only a Chandrasekhar-mass WD accreting H at low rates could be a potential progenitor, while all He-nuclear-burning WDs are ruled out. In the case of SSSs, the upper limits acquired from Remillard et al. (1995) and Farias et al. (2020) are consistent with low and intermediate accretion rates for both H and He accretors, and hence the non-detection of [O III] ionized regions around these sources can potentially be explained within the framework of nuclear-burning WD models embedded in an ambient medium with density close to or lower than 0.2 cm^{-3}. The only exception is RX J0550.0–7151, for which none of the models can explain the lack of the [O III] line, which indicates that the source should be surrounded by an ISM with density substantially lower than 0.2 cm^{-3}.

3.2 Upper limits on the He II 4686 Å surface brightness for SNRs Ia

Additional constraints on the ionizing flux of the SNe Ia progenitor systems have been placed by the Integral Field Unit (IFU) observations carried out by Kuuttila et al. (2019), who searched for He II 4686 Å nebular emission around the three SNRs studied above (0509–67.5, 0519–69.0 and N103B) and the LMC SNR DEM L71. The observations resulted in a non-detection, and thus strict limits were extrapolated on the He II 4686 Å nebular fluxes in the vicinity of the studied remnants (see fifth column of Table 3).

Here, we apply the same method as Kuuttila et al. (2019) to compare our results extracted by CLOUDY with their acquired upper limits. For that reason, we estimate the average surface brightness of the He II 4686 Å emission line in an annulus of 4–5 pc around the SNRs 0509–67.5, N103B and 0519–69.0, and of 7–10 pc around the SNR DEM L71, which correspond to the area ahead of the forward shock in each remnant. In Fig. 5, we plot the upper limits of the He II 4686 Å surface brightness for each object, together with the average surface brightness in the range of 7–10 pc (Fig. 5a–d) and 4–5 pc (Fig. 5e–h) predicted for the H/He nuclear-burning WD models as functions of WD mass and accretion rate and for the two constant ISM densities of 0.2 and 2 cm^{-3}.

As is evident from Fig. 5, almost all of the H/He-accreting WD models lie well above the derived upper limits for the four SNRs in the two density cases of 0.2 and 2 cm^{-3}. There is only a small window where the upper limits for SNRs DEM L71, N103B, and 0519–69.0 are slightly higher than our results in the low-density case and for WD masses $\sim 0.6\,M_\odot$ accreting He-rich matter with high accretion rates (see Fig. 5c and g). Nevertheless, WDs with this mass cannot produce SNe Ia and thus are not of interest here.

In conclusion, even if the limits imposed by the lack of nebular [O III] allow some accreting WD systems to be placed as potential progenitors of the studied SNRs Ia, the non-detection of the He II nebula emission essentially rules out any H/He steadily nuclear-

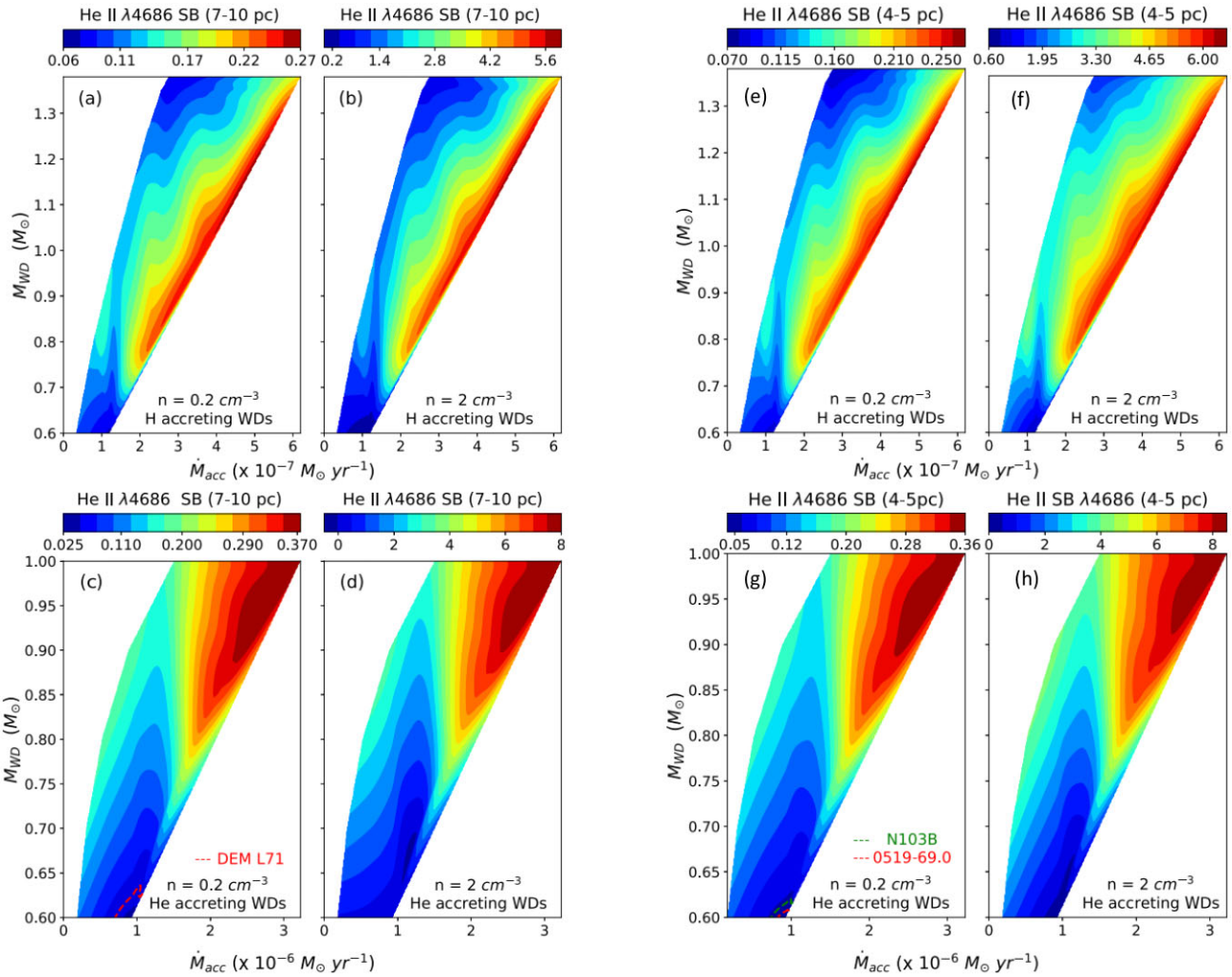

Figure 5. The averaged He II 4686 Å surface brightness in units 10^{-17} erg s^{-1} cm^{-2} arcsec^{-2} at 7–10 pc (a–d) and 4–5 pc (e–h) from the ionizing source, as a function of the accretion rate and the WD mass. The dashed line in (c) represents the upper limit of DEM L71 and those in (g) those of 0519–69.0 and N103B, as extracted by Kuuttila et al. (2019). In the rest of the plots, the upper limits extracted by observations are below the range extracted by our models.

burning WD system in which the accretion process was occurring for about 7×10^4 yr prior the explosion (i.e. the recombination time-scale for helium; Pequignot, Petitjean & Boisson 1991). Alternatively, these remnants could be surrounded by ISM densities much lower than 0.2 cm^{-3}, but such a result is in conflict with their current dynamics and emission properties (Yamaguchi et al. 2014; Martínez-Rodríguez et al. 2018).

3.3 Upper limits from the existence of Balmer-dominated shocks in SNRs Ia

Another restriction on the progenitors of SNe Ia comes from the existence of the Balmer-dominated shocks that are frequently found in SNRs that result – or are suspected to result – from SNe Ia. Their optical spectra show regions that exhibit Balmer line emission with a narrow core and a broad base along the forward shock. Balmer-dominated shocks arise when the forward shock moves into a partially neutral ISM (Chevalier, Kirshner & Raymond 1980). The narrow component is understood to result from collisionally excited neutrals, while the broad component is due to charge exchange (Raymond 2001; Heng 2010, and references therein). As a consequence, the existence of at least some neutral hydrogen in the vicinity of SNRs Ia limits the ionization history of their progenitors to about $\tau_{\rm rec} \sim 10^5$ yr prior to the explosion (Woods et al. 2017, 2018).

In Table 3 (sixth column), we present the minimum required neutral hydrogen fractions, which are consistent with observations and numerical models of the Balmer-dominated shocks (Ghavamian et al. 2002, 2003) associated with two SNRs Ia in our Galaxy (Tycho and SN 1006) and three LMC SNRs Ia (0519–69.0, 0509–67.5 and DEM L71).

With the aim of assessing the limitations imposed by the Balmer shocks on SNe Ia progenitors, in Fig. 6 we present the minimum hydrogen neutral fractions estimated for each SNR Ia of our sample versus its present radius, together with the hydrogen neutral fraction as a function of radial distance from H/He-nuclear-burning WDs of various masses that accrete matter at the two stability limits in the steady accretion regime as extracted by our models.

As Fig. 6 clearly displays, when adopting a surrounding ISM density of 0.2 cm^{-3}, any steady nuclear-burning activity on their WD progenitors is ruled out for $\sim 10^5$ yr prior to the explosion. This result is independent of the assumed WD mass and accretion rate. In the higher-density case ($n_{\rm ism} = 2\,{\rm cm}^{-3}$), He-nuclear-burning

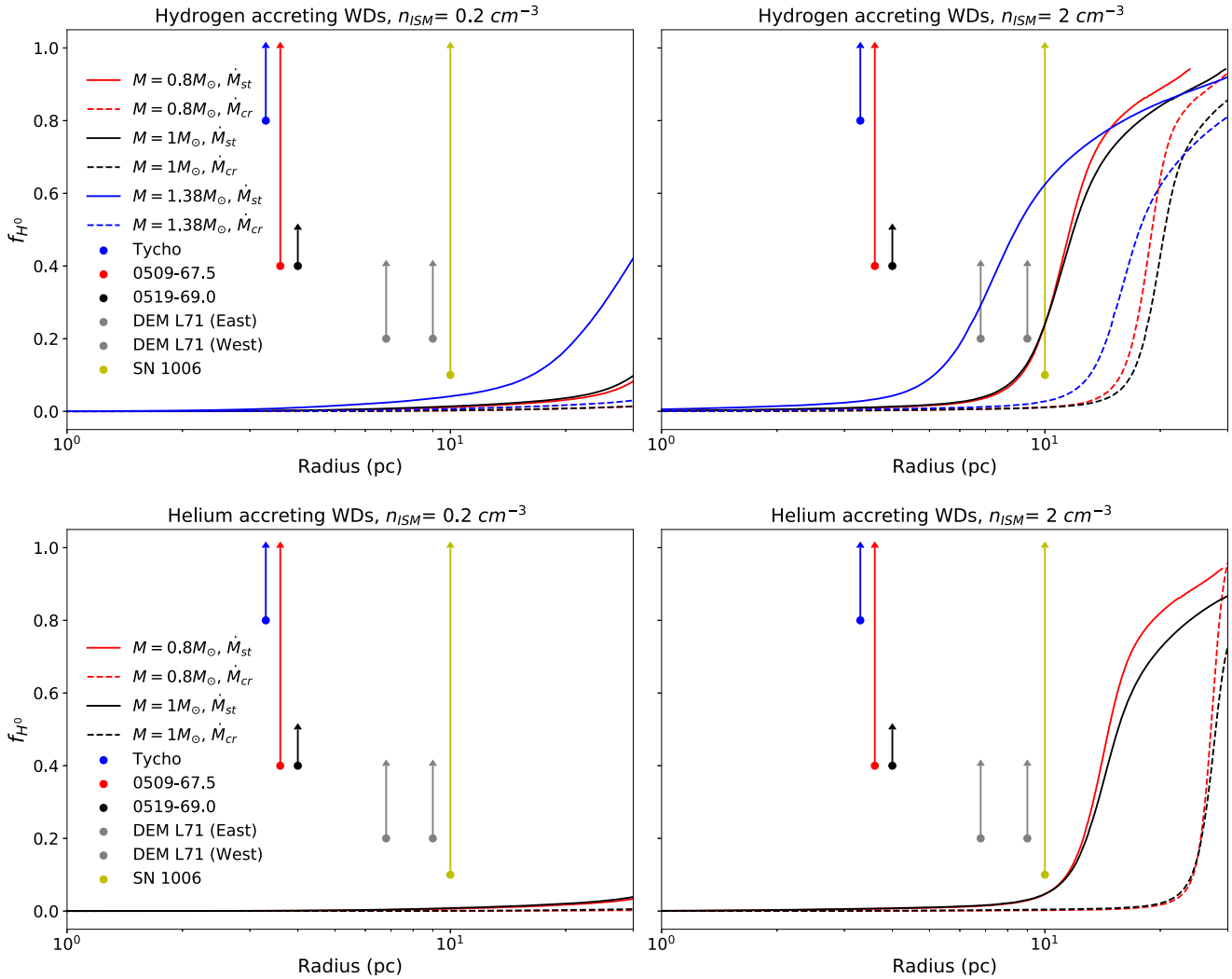

Figure 6. Hydrogen neutral fraction as a function of radial distance from CO WDs accreting H- and He-rich matter at the two stability boundaries in the steady accretion regime for various WD masses. The minimum hydrogen neutral fractions at the present radius of the shock of each remnant are also plotted.

WDs continue to remain inconsistent with the limits acquired from observations, while in the case of H-rich accreted material, WDs accreting matter with low accretion rates cannot be excluded as potential progenitors of SNRs DEM L71 and SN 1006. However, SN 1006 is known to be expanding into a much lower-density medium (see seventh column of Table 3), and in particular its pre-shock gas density has been estimated to be $n_{\rm ism} = 0.25$–$0.4\,{\rm cm}^{-3}$ in the north-western, Balmer-emitting quadrant of the remnant (Raymond et al. 2007).

Summing up, the existence of Balmer-dominated shocks rules out almost any possible stable nuclear-burning WD model (both sub- and Chandrasekhar-mass) that was accreting matter at least $\sim 10^5$ yr prior to the SN Ia explosion. Alternatively, a surrounding ISM with density equal to or higher than 2 $\rm cm^{-3}$ is required. Such a result leads to a fatal problem with to the restrictions imposed by the lack of He II and [O III] bright nebulae around these SNRs, as the latter demand ISM densities close to or lower than 0.2 $\rm cm^{-3}$. Conclusively, any steadily nuclear-burning WD embedded in a constant-density ambient medium seems incapable of satisfying simultaneously the overall observables collected for the studied sample of SNRs, and thus is excluded as a potential SN Ia progenitor for these sources. Such a conclusion stands for any given WD mass and accretion rate, and thus strong limitations are imposed for both the Chandrasekhar-mass and the sub-Chandrasekhar-mass, single-degenerate models of SNe Ia.

4 DISCUSSION

4.1 The imprints of accreting WDs on their ambient medium

In this work, aiming to gain further insights into the interaction of accreting WDs with their ambient medium, we modelled the emission-line spectra of the nebulae around steadily H- and He-nuclear-burning WDs by pairing known WD accretion models with radiation transfer simulations. Having included in our modelling a large range of CO WD masses (0.6–1.38 $\rm M_\odot$ for H-accreting WDs, and 0.6–1.02 $\rm M_\odot$ for He-accreting WDs), all possible accretion rates within the steady accretion regime, and plausible ISM densities, we studied how the ionization state of the gas and the optical nebular emission lines vary with the aforementioned parameters.

Our results show that the level of ionization, the radial extent, and the spectral properties of the formed ionized nebulae vary strongly

with the properties of WD accretion. In particular, we found that the nebulae are expected to be brighter (by about one order of magnitude) and more extended (by a factor of 2) when the mass accretion rate increases from its minimum to its maximum value for a given WD mass. The nebular emission lines are also heavily dependent on the WD mass, with the most extended and brighter nebulae expected around intermediate WD masses ($M_{\rm WD} \sim 0.8$–$1.2\,{\rm M}_{\odot}$). Regarding the chemical composition of the accreted material, we found that He-accreting WDs ionize their ambient medium to larger distances and their nebular emission lines are brighter compared with their H-accreting counterparts.

These results suggest that a great diversity of properties is expected in the medium around steadily accreting WDs, as each nuclear-burning WD leaves its unique and distinctive imprint on the surrounding gas. This is essential in the hunt for accreting WD systems through the detection of their ionized nebulae, given that the optical properties of the ionized gas reveal encoded information about the central source. Our work offers diagnostic tools to enable this information to be deciphered.

Given that accreting WDs are expected to be numerous in every galactic type (van den Heuvel et al. 1992; Rappaport et al. 1994a), it is very unlikely that CAL 83 is the only detected case of a nebula shaped by a WD's accretion activity. Many 'orphan' (without identified ionizing sources), extended ionized nebulae, such as HBW 673 and BCLMP 651 identified in M33 (Kehrig et al. 2011; Woods & Gilfanov 2016), reveal similar properties to those obtained in this work, and, thus, they represent ideal cases to be investigated as possible accreting WD systems. Overall, in agreement with previous studies, we found that the ideal optical line to use in the search for nebulae shaped by accreting WDs is the forbidden line [O III] 5007 Å; we predict this line to be the brightest optical line of the nebulae around most accreting WDs. Nevertheless, our models included an exploration of the forbidden [O II] 3727 Å line that had not been studied previously. We found that in low-density mediums ($n_{\rm ism} \leq 0.2\,{\rm cm}^{-3}$) the [O III] 5007 Å line is very reduced, and the most prominent line becomes the [O II] 3727 Å one. Thus, this line could potentially be useful in observational searches for accreting WD nebulae, especially if these sources are embedded in mediums with low ambient densities. Moreover, other bright and dominant optical signatures of the nebulae formed around accreting WDs are expected to be the Hα, [N II] 6584 Å and [S II] 6717 Å emission lines, as they are the other brightest lines among the emission lines studied in all of our models. Finally, regarding the likelihood of the detection of accreting WDs through their ionized nebulae, our modelling has shown that intermediate-mass WDs ($M_{\rm WD} \sim 0.8$–$1.2\,{\rm M}_{\odot}$) that accrete steadily at the maximum possible range ($\dot{M}_{\rm acc} \sim \dot{M}_{\rm cr}$) have a higher probability of being identified because they produce the most extended and bright nebulae. The same applies for the He-accreting WDs (compared with their H-accreting counterparts) because they tend to be hotter and more luminous ionizing sources.

To further untangle the expected imprints of steadily accreting WDs compared with other ionizing sources, we explored how the extracted nebular line-emission ratios fit to various diagnostic diagrams used to separate and characterize emission-line objects. Our findings agree with those extracted by Rappaport et al. (1994b), showing that the nebulae around accreting WDs are clearly distinctive compared with those of typical H II regions. In particular, all nebulae produced by our models possess [N II] λ6584, [S II] λ6717, 31 and [O I] λ6300 over Hα ratios that are much higher than those produced by young massive stars. However, there is some contamination between the properties of the two objects, in that for the case of highly accreting, low-mass WDs ($M_{\rm WD} \leq 0.6\,{\rm M}_{\odot}$), the formed nebulae are expected to have properties similar to those of H II-like objects. Rappaport et al. (1994b) focused on hot, luminous, accreting WDs – expected to be members of the SSS class – and argued that the [O III] λ5007/Hβ ratio can be used as a distinctive diagnostic tool between the nebulae around massive accreting WDs and H II regions, as the line ratio values in their supersoft models were much higher than those in H II regions. However, considering the whole range of accreting WDs, this argument is no longer valid, as we found that the ranges of the [O III] λ5007/Hβ ratio for the H II regions and steadily nuclear-burning WD nebulae overlap significantly. Thus, the lower ionization lines [N II] λ6584, [S II] λ6717, 31 and [O I] λ6300 compared with Hα seem a safer diagnostic tool for the two classes of ionized nebulae. Another distinctive consequence of our broader and more realistic modelling is the extraction of a much wider range for nebula line ratios than inferred by previous works. This is important in the context of ionized nebulae around accreting WDs, because, for most of the ions, the previous theoretical SSS models predict much higher line ratios (compared with Hβ) than were observed by Gruyters et al. (2012), and the models did not have a convincing explanation for these systematic discrepancies. The response of the WD to mass accretion seems to be able to account for such variances. Some examples include the [O III]/Hβ and [N II]/Hβ ratios, which are much lower in our models and in better agreement with CAL 83 observations.

Finally, an additional interesting finding derived from the BPT diagrams of our models is that the vast majority of nebulae around H- and He-nuclear-burning WDs coincide with the loci of the galactic LIERs. The origin of LIERs has been attributed to the ionization produced by the activity of a low-luminosity AGNs (Ferland & Netzer 1983). However, the discovery of spatially extended LIERs (Macchetto et al. 1996; Gomes et al. 2016) implies ionization by an extended component that follows a stellar-like radial distribution (Singh et al. 2013). Until now, it had been suggested that the only viable extended sources of ionizing photons for passively evolving galaxies were hot post-asymptotic giant branch (AGB) stars (Singh et al. 2013; Byler et al. 2019). Our models indicate that steadily accreting WDs – especially those that accrete H-rich material – could be an alternative/additional source of LIERs, as they seem to produce nebulae that have the same spectroscopic properties. Similar to post-AGB stars, accreting WDs are expected to be hosted in copious amounts in galaxies of all morphological types, which could potentially explain why LIERs are mostly found in galaxies with old populations and that display little or no star-formation activity. On the other hand, the fact that the lifespan of accreting WDs can be orders of magnitude larger than the short-lived post-AGB phase means that the former are more persistent, and thus are more efficient ionizing sources. The same applies for the diffuse ionized gas (DIG, Reynolds 1984; Haffner et al. 2009) and especially for its HOLMES (hot low-mass evolved stars) component, whose emission flux ratios are nearly always consistent with the LIER loci in BPT diagrams (e.g. Kumari et al. 2019). Steadily accreting WDs could potentially contribute to the formation of these nebulae together with the post-AGB stars that to date have been proposed to be their ionizing source (e.g. Byler et al. 2019). However, even if this explanation is tempting, in order to draw a firm conclusion on the contribution of steadily accreting WDs to LIER/DIG formation, detailed radiation transfer simulations coupled with binary population synthesis techniques are required.

4.2 Comparing the results of our modelling with the relevant observations

In the section 3 of this paper, we compared the results extracted by our radiation transfer simulations with the relevant observables we received from the vicinity of accreting WD systems and related objects. The aim of this comparison was to (re)assess – with broader and more detailed modelling – whether the theoretical predictions on the ionizing flux from steadily accreting WDs are aligned with the lack of any ionized nebulae around the most massive members of their class, namely the SSSs, and subsequently to investigate if steadily nuclear-burning WDs could be the progenitors of a number of well-studied SNRs Ia.

Regarding the SSSs, our modelling has shown that the non-detection of [O III]-bright ionized regions around the nine studied SSSs in the LMC/SMC establishes an upper limit for their ambient medium densities equal or close to 0.2 cm^{-3}, while for the case of the SSS RX J0550.0–7151 a lower-density ambient medium is required. These constraints on the ISM density around the studied SSSs are the strictest compared with the relevant ones in the current literature (Woods et al. 2017; Farias et al. 2020) and are applied for any possible combination of WD mass and accretion rate within the stable accretion regime.

The demand for an ambient medium around the studied SSSs with density well below 0.2 cm^{-3} contradicts the general expectations, given that the typical range of LMC midplane densities is $n_0 \approx 0.1$–4 cm^{-3}, while the ISM densities around these sources have been estimated to be $n_{sss} = 0.22$–$2.26\,cm^{-3}$, based on the total H I column density in the direction of each source and assuming an isothermal disc distribution (Woods & Gilfanov 2016). However, hot and very low-density ISM densities are met in the LMC/SMC and are linked to the hot supernova-heated component (Cox 2005). Thus, there is still the possibility of a 'natural coincidence' under which all studied SSSs, except CAL 83, are embedded in the most tenuous regions of their host galaxy.

This scenario is not applicable for the case of the studied SNRs Ia. The observational pieces of evidence involved in our study, namely the lack of nebular [O III] and He II emission around the SNRs Ia and the existence of Balmer lines in their shock waves, act together to exclude stably accreting WDs as possible progenitor systems. In particular, the absence of detected [O III] and He II nebulae in the vicinity of SNRs Ia excludes all stable nuclear-burning WDs for ISM densities of $n_{ism} > 0.2\,cm^{-3}$, while the existence of Balmer-dominated shocks is inconsistent for ISM densities of $n_{ism} < 2\,cm^{-3}$. Thus, within the steady accretion regime and for both H- and He-accreting WDs, there is no possible combination of WD mass, accretion rate and ISM density capable of reproducing simultaneously the two observational facts that the SNRs Ia impose. This result essentially rules out any WD that was steadily burning the accreted matter $\sim 10^5$ yr before its final explosion as a possible progenitor of the studied remnants, and therefore challenges both the Chandrasekhar- and sub-Chandrasekhar-mass scenarios arising from single-degenerate progenitors. Inevitably, the double-degenerate scenario is positioned as the most plausible origin of the studied remnants.

Nevertheless, such a bold statement is possibly in tension with a number of findings that indicate that some of the studied SNRs might have originated from a single-degenerate SN Ia (see Maoz, Mannucci & Nelemans 2014; Livio & Mazzali 2018, for an extensive discussion and references therein), and thus, before drawing a final conclusion, some possible caveats need to be addressed in order to achieve a holistic picture that emerges by combining the observations and the contrasting, relevant theoretical predictions. Some of them, already discussed in the literature, refer to a 'time window' between the WD accretion phase and the final SN Ia explosion. If this time interval is longer than the recombination time-scale of the surrounding nebula, then at the moment of the explosion the surrounding gas will have recombined, returning into its (partially) neutral state. This time delay can be achieved through the so-called 'simmering phase' (Martínez-Rodríguez et al. 2016; Piersanti et al. 2017), the 'spin-up/spin-down' WD model (Di Stefano, Voss & Claeys 2011), as well as in the sub-Chandrasekhar edge-lit detonation models, where the WD spends a substantial amount of time in the helium detonation regime (see Fig. 1) before its fatal explosion (Ruiter et al. 2011). All the above scenarios, plausible or not, could offer the desired time delay as long as mass accretion ceases during this period.

Another possible parameter that we could question is whether the accreting WD progenitors were indeed embedded in a homogeneous ambient medium. Given that SNe Ia result from intermediate-mass stars, no substantial modifications are expected to occur from their progenitor systems. Indeed, the overall morphological (Lopez et al. 2009) and X-ray (Badenes et al. 2007; Yamaguchi et al. 2014) properties of SNRs Ia indicate that these objects are evolving in a rather homogeneous ambient medium. However, detailed studies of individual SNRs Ia have shown that their explosion centres were surrounding by moderate circumstellar structures, and currently the remnants are interacting with them or they had an interaction history with them in the recent past. Such cases are, for instance, the young remnants of Kepler's SNR (Chiotellis, Schure & Vink 2012; Burkey et al. 2013; Toledo-Roy et al. 2014), Tycho's SNR (Dwarkadas & Chevalier 1998; Katsuda et al. 2010; Chiotellis et al. 2013), G1.9+0.3 (Borkowski et al. 2013, 2017; Chiotellis, Boumis & Spetsieri 2021), RCW86 (Williams et al. 2011; Broersen et al. 2014), N103B (Li et al. 2017; Yamaguchi et al. 2021) and the more evolved ones of DEM L238 and DEM L249 (Borkowski, Hendrick & Reynolds 2006) etc. Recently, the detection of numerous high-density knots around the LMC remnants 0519–69.0, N103B, DEM L71, and 0548–70.4 have also been associated with a circumstellar medium (CSM) ejected by the SN progenitor system (Li et al. 2021). Such circumstellar structures can be formed by the mass outflows of the progenitor system as it is evolving towards a SN Ia. The formation of the WD itself requires the ejection of the stellar hydrogen-rich envelope during the planetary nebula phase or by a common-envelope episode. The ejected envelope itself is capable of forming extended circumstellar structures around the binary system with lifetimes up to several Myr (Chiotellis, Boumis & Spetsieri 2020). In addition, the ionizing flux produced by accreting WDs leads to an overpressure of the heated ambient gas that results in the expansion of the surrounding nebula and the formation of non-homogeneous bubbles around the binary system (Rappaport et al. 1994b). A modified, non-homogeneous ambient medium around the accreting WD will substantially alter the ionization and emission properties of the resulting nebula, and thus it can serve as an additional possible solution for the lack of an ionized region around the studied SNRs Ia. Note that this scenario is also applicable for the non-detection of ionized nebulae around the studied SSSs for which the 'time window' scenario discussed above is not valid because for these objects accretion is an ongoing process.

However, detailed radiation transfer modelling is required to assess if indeed such circumstellar structures can offer a plausible explanation of the current observables we receive from SSSs and SNRs, and, if so, to identify the properties and the origin of these structures (Souropanis et al. in preparation).

5 SUMMARY

In this paper we have studied the observational imprints that steadily accreting WDs leave on their ambient medium owing to their ionizing activity. By coupling known H- and He-accreting WD models with radiation transfer simulations, we extracted the sizes, optical line luminosities and surface-brightness profiles of the surrounding ionizing gas as a function of the WD mass and accretion rate, the ISM density, and the chemical composition of the accreted material.

Our results have shown that all accreting WDs are efficient ionizing sources capable of forming extended, optical-bright nebulae in their vicinity. The most efficient sources were found to be intermediate-mass accreting WDs ($M_{\rm WD} \approx 0.8$–$1.2\,{\rm M}_{\odot}$) that accrete mass at the maximum possible rate of the steady accretion regime. These sources form the largest and brightest nebulae around them and thus are more likely to be detected. The same applies for He-accreting WDs as, compared with their H-accreting counterparts, they appear to be hotter and more luminous sources and thus more efficient ionizing sources. Overall, the ionization and emission properties of the formed nebulae are strongly dependent on the accretion properties of the central WD. That means that each accreting WD, for a given mass and accretion rate, forms an ionized nebula around it characterized by unique and distinctive properties. Thus, through our modelling we provide direct links through which the emission properties of the surrounding nebula can be encoded, revealing the nature and the properties of the central source.

The formed ionized nebulae represent efficient tools for detecting steadily accreting WDs, as in most cases the source itself is utterly obscured. Among the studied recombination and forbidden lines, we found that the most luminous ones are [O III] 5007 Å and [O II] 3727 Å, the latter being the dominant one in low-density environments. Thus, these two oxygen lines are ideal traces for the detection of ionized nebulae around accreting WDs. Other lines in which the ionized gas around steadily accreting WDs is expected to be bright are those of Hα, [N II] 6584 Å and [S II] 6717 Å.

We displayed our results on so-called BPT diagrams and found that the nebulae formed by accreting WDs reveal properties that are distinct from H II-like regions, possessing higher [N II] λ6584, [S II] λ6717, 31 and [O I] λ6300 over Hα ratios. However, some contamination in the line ratios exists between the two objects for the case of highly accreting low-mass WDs ($M_{\rm WD} \leq 0.6\,{\rm M}_{\odot}$). Intriguingly, the majority of the nebulae formed by steadily nuclear-burning WDs have the same optical line ratio properties as those observed in galaxies that exhibit LIERs. We suggest that accreting WDs, being numerous in any galactic type, could potentially be one of the main contributors to the formation of LIERs.

Finally, we compared the results extracted by our theoretical modelling with the relevant observations conducted in the vicinity of a number of SSSs and SNRs Ia. We found that the non-detection of any ionized optical nebula around all studied SSSs, with the exception of CAL 83, establishes an upper limit on their ambient medium density equal to 0.2 cm^{-3}. Regarding the studied SNRs, we found that the lack of nebular [O III] and He II emission in the vicinity of their forward shocks in combination with the existence of Balmer-dominated lines mutually excludes any accreting WD progenitor that was steadily burning the accreted material $t \sim 10^5$ yr before the SN Ia explosion. This result concerns any single-degenerate accretion model, including the canonical Chandrasekhar and the sub-Chandrasekhar mass models (WD + helium-rich donor star channels). We discussed possible alternatives that could potentially eliminate any possible discrepancies between the predictions of the single-degenerate models and the relevant observables. We claim that a plausible solution would be the consideration of a non-homogeneous ambient medium around the SN Ia explosion centre, modified either by the mass outflows of the progenitor system or/and by the ionizing radiation produced by the accreting WD.

ACKNOWLEDGEMENTS

The authors would like to thank the referee for their thorough comments that improved the manuscript. This research is co-financed by Greece and the European Union (European Social Fund, ESF) through the Operational Programme 'Human Resources Development, Education and Lifelong Learning 2014-2020' in the context of the project 'On the Interaction of Type Ia Supernovae with Planetary Nebulae' (MIS 5049922). AC acknowledges support of this work by the project 'PROTEAS II' (MIS 5002515), which is implemented under the Action 'Reinforcement of the Research and Innovation Infrastructure', funded by the Operational Programme 'Competitiveness, Entrepreneurship and Innovation' (NSRF 2014-2020) and co-financed by Greece and the European Union (European Regional Development Fund). MC acknowledges support by NSF (1910687), NASA (19-ATP19-0188), and STScI (*HST*-AR-14556.001-A). LP acknowledges partial financial support from the INAF-mainstream project 'Type Ia Supernovae and their Parent Galaxies: Expected Results from LSST. AJR is supported by an Australian Research Council Future Fellowship through award number FT170100243. GF acknowledges support by NSF (1816537, 1910687), NASA (ATP 17-ATP17-0141, 19-ATP19-0188), and STScI (*HST*-AR- 15018 and *HST*-GO-16196.003-A).

DATA AVAILABILITY

The data underlying this article will be shared on reasonable request to the corresponding author.

REFERENCES

Acero F., Ballet J., Decourchelle A., 2007, A&A, 475, 883
Akras S., Guzman-Ramirez L., Leal-Ferreira M. L., Ramos-Larios G., 2019, ApJS, 240, 21
Allende Prieto C., Lambert D. L., Asplund M., 2001, ApJ, 556, L63
Badenes C., Borkowski K. J., Hughes J. P., Hwang U., Bravo E., 2006, ApJ, 645, 1373
Badenes C., Hughes J. P., Bravo E., Langer N., 2007, ApJ, 662, 472
Baldwin J. A., Phillips M. M., Terlevich R., 1981, PASP, 93, 5
Borkowski K. J., Hendrick S. P., Reynolds S. P., 2006, ApJ, 652, 1259
Borkowski K. J., Reynolds S. P., Hwang U., Green D. A., Petre R., Krishnamurthy K., Willett R., 2013, ApJ, 771, L9
Borkowski K. J., Gwynne P., Reynolds S. P., Green D. A., Hwang U., Petre R., Willett R., 2017, ApJ, 837, L7
Broersen S., Chiotellis A., Vink J., Bamba A., 2014, MNRAS, 441, 3040
Burkey M. T., Reynolds S. P., Borkowski K. J., Blondin J. M., 2013, ApJ, 764, 63
Byler N., Dalcanton J. J., Conroy C., Johnson B. D., Choi J., Dotter A., Rosenfield P., 2019, AJ, 158, 2
Cassisi S., Iben Icko J., Tornambè A., 1998, ApJ, 496, 376
Chen H.-L., Woods T. E., Yungelson L. R., Gilfanov M., Han Z., 2015, MNRAS, 453, 3024
Chevalier R. A., Kirshner R. P., Raymond J. C., 1980, ApJ, 235, 186
Chiotellis A., Schure K. M., Vink J., 2012, A&A, 537, A139
Chiotellis A., Kosenko D., Schure K. M., Vink J., Kaastra J. S., 2013, MNRAS, 435, 1659
Chiotellis A., Boumis P., Spetsieri Z. T., 2020, Galaxies, 8, 38

Chiotellis A., Boumis P., Spetsieri Z. T., 2021, MNRAS, 502, 176
Choudhury S., Subramaniam A., Cole A. A., Sohn Y. J., 2018, MNRAS, 475, 4279
Cox D. P., 2005, ARA&A, 43, 337
Di Stefano R., Voss R., Claeys J. S. W., 2011, ApJ, 738, L1
Dwarkadas V. V., Chevalier R. A., 1998, ApJ, 497, 807
Farias D. A., Clocchiatti A., Woods T. E., Rest A., 2020, MNRAS, 497, 3234
Ferland G. J., Netzer H., 1983, ApJ, 264, 105
Ferland G. J. et al., 2017, Rev. Mex. Astron. Astrofis., 53, 385
Fink M., Röpke F. K., Hillebrandt W., Seitenzahl I. R., Sim S. A., Kromer M., 2010, A&A, 514, A53
Gallagher J. S., Starrfield S., 1978, ARA&A, 16, 171
Ghavamian P., Raymond J., Smith R. C., Hartigan P., 2001, ApJ, 547, 995
Ghavamian P., Winkler P. F., Raymond J. C., Long K. S., 2002, ApJ, 572, 888
Ghavamian P., Rakowski C. E., Hughes J. P., Williams T. B., 2003, ApJ, 590, 833
Ghavamian P., Blair W. P., Sankrit R., Raymond J. C., Hughes J. P., 2007, ApJ, 664, 304
Gomes J. M. et al., 2016, A&A, 588, A68
Graur O., Woods T. E., 2019, MNRAS, 484, L79
Grevesse N., Sauval A. J., 1998, Space Sci. Rev., 85, 161
Gruyters P., Exter K., Roberts T. P., Rappaport S., 2012, A&A, 544, A86
Hachisu I., Kato M., Nomoto K., Umeda H., 1999, ApJ, 519, 314
Haffner L. M. et al., 2009, Reviews of Modern Physics, 81, 969
Heng K., 2010, PASA, 27, 23
Hillebrandt W., Kromer M., Röpke F. K., Ruiter A. J., 2013, Frontiers Phys, 8, 116
Holberg J. B., 2009, J. Phys. Conf. Ser., 172, 012022
Holweger H., 2001, in Wimmer-Schweingruber R. F., ed., AIP Conf. Ser. Vol. 598, Joint SOHO/ACE workshop 'Solar and Galactic Composition'. AIP, Melville, NY, p. 2
Iben I. J., Tutukov A. V., 1984, ApJS, 54, 335
Kahabka P., van den Heuvel E. P. J., 1997, ARA&A, 35, 69
Kato T., Kanatsu K., Takamizawa K., Takao A., Stubbings R., 2000, IAU Circ., 7552, 1
Katsuda S., Petre R., Hughes J. P., Hwang U., Yamaguchi H., Hayato A., Mori K., Tsunemi H., 2010, ApJ, 709, 1387
Kauffmann G. et al., 2003, MNRAS, 346, 1055
Kehrig C. et al., 2011, A&A, 526, A128
Kemp A. J., Karakas A. I., Casey A. R., Izzard R. G., Ruiter A. J., Agrawal P., Broekgaarden F. S., Temmink K. D., 2021, MNRAS, 504, 6117
Kewley L. J., Dopita M. A., Sutherland R. S., Heisler C. A., Trevena J., 2001, ApJ, 556, 121
Kewley L. J., Groves B., Kauffmann G., Heckman T., 2006, MNRAS, 372, 961
Kosenko D., Vink J., Blinnikov S., Rasmussen A., 2008, A&A, 490, 223
Kosenko D., Ferrand G., Decourchelle A., 2014, MNRAS, 443, 1390
Kumari N., Maiolino R., Belfiore F., Curti M., 2019, MNRAS, 485, 367
Kuuttila J., Gilfanov M., Seitenzahl I. R., Woods T. E., Vogt F. P. A., 2019, MNRAS, 484, 1317
Lewis K. T., Burrows D. N., Hughes J. P., Slane P. O., Garmire G. P., Nousek J. A., 2003, ApJ, 582, 770
Li C.-J. et al., 2017, ApJ, 836, 85
Li C.-J., Chu Y.-H., Raymond J. C., Leibundgut B., Seitenzahl I. R., Morlino G., 2022, AAS, 926, 207
Li X. D., van den Heuvel E. P. J., 1997, A&A, 322, L9
Livio M., Mazzali P., 2018, Phys. Rep., 736, 1
Livne E., 1990, ApJ, 354, L53
Lopez L. A., Ramirez-Ruiz E., Badenes C., Huppenkothen D., Jeltema T. E., Pooley D. A., 2009, ApJ, 706, L106
Macchetto F., Pastoriza M., Caon N., Sparks W. B., Giavalisco M., Bender R., Capaccioli M., 1996, A&AS, 120, 463
Madej J., Należyty M., Althaus L. G., 2004, A&A, 419, L5
Maoz D., Mannucci F., Nelemans G., 2014, ARA&A, 52, 107
Martínez-Rodríguez H., Piro A. L., Schwab J., Badenes C., 2016, ApJ, 825, 57
Martínez-Rodríguez H. et al., 2018, ApJ, 865, 151
Mikołajewska J., 2007, Baltic Astron., 16, 1
Mohamed S., Podsiadlowski P., 2012, Baltic Astron., 21, 88
Nelemans G., Yungelson L. R., Portegies Zwart S. F., Verbunt F., 2001, A&A, 365, 491
Nomoto K., Saio H., Kato M., Hachisu I., 2007, ApJ, 663, 1269
Osterbrock D. E., Ferland G. J., 2006, Astrophysics of gaseous nebulae and active galactic nuclei
Paczyński B., 1967, Acta Astron., 17, 287
Pequignot D., Petitjean P., Boisson C., 1991, A&A, 251, 680
Piersanti L., Tornambé A., Yungelson L. R., 2014, MNRAS, 445, 3239
Piersanti L., Yungelson L. R., Tornambé A., 2015, MNRAS, 452, 2897
Piersanti L., Bravo E., Cristallo S., Domínguez I., Straniero O., Tornambé A., Martínez-Pinedo G., 2017, ApJ, 836, L9
Piro A. L., Thompson T. A., Kochanek C. S., 2014, MNRAS, 438, 3456
Rakowski C. E., Ghavamian P., Hughes J. P., 2003, ApJ, 590, 846
Rappaport S., Di Stefano R., Smith J. D., 1994a, ApJ, 426, 692
Rappaport S., Chiang E., Kallman T., Malina R., 1994b, ApJ, 431, 237
Raymond J. C., 2001, Space Sci. Rev., 99, 209
Raymond J. C., Korreck K. E., Sedlacek Q. C., Blair W. P., Ghavamian P., Sankrit R., 2007, ApJ, 659, 1257
Remillard R. A., Rappaport S., Macri L. M., 1995, ApJ, 439, 646
Rest A. et al., 2005, Nature, 438, 1132
Reynolds R. J., 1984, ApJ, 282, 191
Ruiter A. J., 2020, IAU Symp., 357, 1
Ruiter A. J., Belczynski K., Sim S. A., Hillebrandt W., Fryer C. L., Fink M., Kromer M., 2011, MNRAS, 417, 408
Schawinski K., Thomas D., Sarzi M., Maraston C., Kaviraj S., Joo S.-J., Yi S. K., Silk J., 2007, MNRAS, 382, 1415
Seitenzahl I. R., Ghavamian P., Laming J. M., Vogt F. P. A., 2019, Phys. Rev. Lett., 123, 041101
Shen K. J., Bildsten L., 2007, ApJ, 660, 1444
Shen K. J., Kasen D., Miles B. J., Townsley D. M., 2018, ApJ, 854, 52
Sim S. A., Röpke F. K., Hillebrandt W., Kromer M., Pakmor R., Fink M., Ruiter A. J., Seitenzahl I. R., 2010, ApJ, 714, L52
Singh R. et al., 2013, A&A, 558, A43
Tian W. W., Leahy D. A., 2011, ApJ, 729, L15
Toledo-Roy J. C., Esquivel A., Velázquez P. F., Reynoso E. M., 2014, MNRAS, 442, 229
Toonen S., Hollands M., Gänsicke B. T., Boekholt T., 2017, A&A, 602, A16
van den Heuvel E. P. J., Bhattacharya D., Nomoto K., Rappaport S. A., 1992, A&A, 262, 97
Warren J. S., Hughes J. P., 2004, ApJ, 608, 261
Whelan J., Iben Icko J., 1973, ApJ, 186, 1007
Williams B. J. et al., 2011, ApJ, 741, 96
Williams B. J., Borkowski K. J., Ghavamian P., Hewitt J. W., Mao S. A., Petre R., Reynolds S. P., Blondin J. M., 2013, ApJ, 770, 129
Williams B. J. et al., 2014, ApJ, 790, 139
Wolf W. M., Bildsten L., Brooks J., Paxton B., 2013, ApJ, 777, 136
Woods T. E., Gilfanov M., 2016, MNRAS, 455, 1770
Woods T. E., Ghavamian P., Badenes C., Gilfanov M., 2017, Nature Astron., 1, 800
Woods T. E., Ghavamian P., Badenes C., Gilfanov M., 2018, ApJ, 863, 120
Woosley S. E., Kasen D., 2011, ApJ, 734, 38
Yamaguchi H. et al., 2014, ApJ, 785, L27
Yamaguchi H., Acero F., Li C.-J., Chu Y.-H., 2021, ApJ, 910, L24

APPENDIX A: MODELLING IONIZED NEBULAE AROUND ACCRETING WDS

In this appendix, we provide, for the sake of the reproducibility of our results, a minimal CLOUDY input script that we used to simulate the ionized nebulae around steadily nuclear-burning accreting WDs. In this example, we model the nebula ionized by a 1-solar-mass WD accreting H-rich matter with $\dot{M}_{\rm st}$, for an ISM density of 2 cm^{-3} and solar gas abundances.

```
blackbody, T = 524807.46 K
luminosity linear solar 10000
hden 2 linear
abundances 'default.abn'
radius 16
sphere
iterate
stop temperature 3e3K
save lines, emergent emissivity, 'lines.str' last
O 3 5006.84A
O 2 3728.81A
O 2 3726.03A
O 1 6300.30A
H 1 4861.33A
H 1 6562.81A
N 2 6583.45A
He 2 4685.64A
end of lines
```

This paper has been typeset from a TEX/LATEX file prepared by the author.